Physics and Imaging in Radiation Oncology 14 (2020) 12–16

Contents lists available at ScienceDirect

Physics and Imaging in Radiation Oncology

journal homepage: www.elsevier.com/locate/phro

Original Research Article

Impact of radiopacified bone cement on radiotherapy dose calculation

Scott B. Crowe[a,b,c,*], Jane Bennett[a], Marika Lathouras[a], Craig M. Lancaster[a], Steven R. Sylvander[a], Benjamin Chua[a,d], Catherine S. Bettington[a,d], Charles Y. Lin[a,d], Tanya Kairn[a,b]

[a] Cancer Care Services, Royal Brisbane & Women's Hospital, Herston, QLD 4029, Australia
[b] Science and Engineering Faculty, Queensland University of Technology, Brisbane, QLD 4000, Australia
[c] Herston Biofabrication Institute, Herston, QLD 4029, Australia
[d] Faculty of Medicine, University of Queensland, St. Lucia, QLD 4072, Australia

ARTICLE INFO

Keywords:
Radiation therapy
Treatment planning
Cranioplasty
Bone cement

ABSTRACT

Background and purpose: Radiopacifiers are introduced to bone cements to provide the appearance of bone in kilovoltage (kV) radiographic images. For higher energy megavoltage (MV) radiotherapy treatment beams, however, these radiopacifiers do not cause a bone-like perturbation of dose. This study therefore aimed to determine the impact of the barium-contrasted plastic-based cement materials on radiotherapy dose calculations.

Materials and methods: The radiological properties of a physical sample of bone cement were characterised by computed tomography (CT) imaging and transmission measurements. Monte Carlo simulations of percentage depth-dose profiles were performed to determine the possible dose error for MV treatment beams. Dose differences were then investigated for clinical volumetric modulated radiotherapy treatment plans, with and without density overrides applied.

Results: Differences of up to 7% were observed at the downstream interface of a 0.6 cm thick bone cement layer, compared to bone. Differences in planning target volume dose-volume metrics varied between −0.5% and 2.0%.

Conclusion: Before planning radiotherapy treatments for patients who have undergone cranioplasty, every effort should be made to identify whether a radiopacified bone cement has been implanted. Density overrides should be applied to minimise dose calculation errors, whenever bone cement is used.

1. Introduction

Plastic-based bone cements are a commonly used cranioplasty material, used in the surgical repair of cranial defects, particularly when sections of the skull bone must be excised due to tumour involvement. Plastic-based bone cements often include a radiopacifying additive (or contrast agent), to provide a degree of X-ray opacity, to allow the orthopaedic surgeon to monitor healing processes or fatigue fractures [1]. For patients undergoing computed tomography (CT) simulation for radiation therapy treatments, these cements may appear as typical bone.

The most commonly used radiopacifier additives in bone cements are barium sulphate ($BaSO_4$) and zirconium dioxide (ZrO_2), which are used in concentrations of 8–15% [1,2]. The attenuation provided by these additives is dependent on photon energy, due to variations in physical cross sections; specifically, the photoelectric effect dominates at kilovoltage (kV) imaging energies, while Compton scattering dominates at megavoltage (MV) treatment energies. The radiopacifiers can therefore cause potential issues for radiotherapy treatment planning, delivery and quality assurance, because radiopacified materials that appear as dense as bone in kV images actually behave as though closer to unit density when irradiated using MV treatment beams. The impact of barium sulfate contrast agents on dose calculations has been discussed with respect to 3D printed radiotherapy quality assurance phantoms [3], contrasted bolus [4] and intravenous CT contrast agents [5], but has not previously been addressed in regard to bone cements used in cranioplasty.

There is therefore a risk of error in dose delivery in patients presenting with plastic-based bone cements if the cement is mistaken for bone in the planning CT image and these additives are not appropriately handled within the treatment planning system (e.g. through the use of density overrides).

This study therefore evaluated the radiological properties of plastic-based bone cements containing barium sulphate and characterised the impact of cranial barium-contrasted plastic-based cement implants on the accuracy of radiotherapy dose calculations.

* Corresponding author.
E-mail address: sb.crowe@gmail.com (S.B. Crowe).

https://doi.org/10.1016/j.phro.2020.04.004
Received 21 February 2020; Received in revised form 22 April 2020; Accepted 29 April 2020

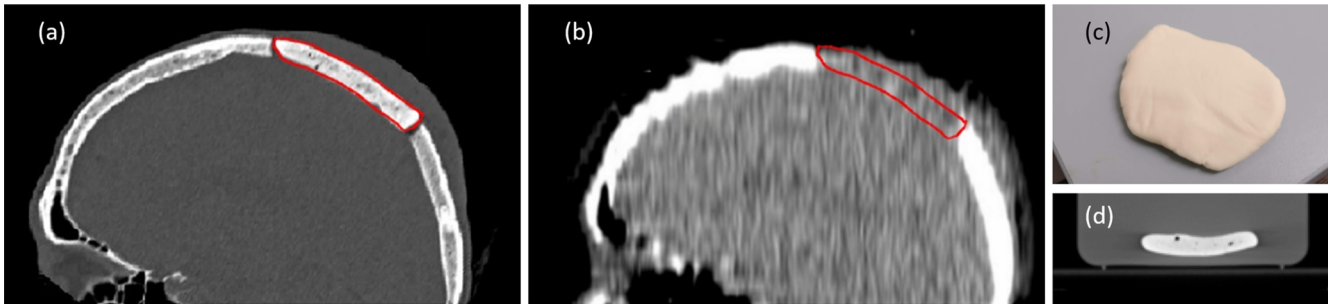

Fig. 1. One patient's barium-contrasted plastic-based cement implant (contoured in red), imaged with (a) nominal 100 kVp CT and (b) nominal 3.5 MV CT, alongside (c) a photograph and (d) a nominal 120 kVp CT of the bone cement sample used in this work.

2. Material and methods

2.1. Radiodensity characterisation

Fig. 1 provides an example of how the differing effects of radiopacified bone cements can manifest, for kV and MV photon beams. Fig. 1(a) and (b) respectively show kV and MV images acquired for the same patient, showing the same barium-contrasted plastic-based cement implant. The effect of the near-unit density of the bone cement is apparent in its tissue-equivalent appearance in the MV CT image (Fig. 1(b)). The magnitude of this effect was investigated using several methods to characterize the radiodensity of a physical sample of DePuy CMW 1 Gentamicin (DePuy Synthes, Raynham, USA) bone cement, shown in Fig. 1(c) and (d), as described below.

First, the mass density, ρ, and relative electron density (the electron density relative to water, $\rho_e/\rho_{e,w}$, also known as RED) were determined by CT imaging the bone cement sample using two systems: a Siemens SOMATOM Confidence CT scanner (Siemens AG, Erlangen, Germany), operating at a peak tube potential 120 kVp with an exposure of 260 mAs; and a TomoTherapy Hi-Art unit (Accuray Inc, Sunnyvale, USA), operating at a peak imaging beam energy of approximately 3.5 MVp. CT-derived ρ and $\rho_e/\rho_{e,w}$ values were calculated by interpolation of CT number to density calibration data for these scanners, acquired by imaging of a Gammex Model 467 tissue characterisation phantom (Gammex Inc., Middleton, USA).

After observing that the MV CT produced dramatically different radiodensity results from the kV CT of the sample (see Section 3.1), additional radiodensity measurements were performed using a narrow (3×3 cm^2) 6 MV radiotherapy beam from a Varian Clinac 21iX (Varian Medical Systems, Palo Alto, USA), to investigate the consistency of results between using the MV CT imaging system and the MV treatment beam. A method described by Moutrie et al. [6] was used to identify the "effective" relative electron density, $(\rho_e/\rho_{e,w})_{eff}$, which is the $\rho_e/\rho_{e,w}$ of the sample as identified using an electronic portal imaging device (EPID), for the particular therapy beam and the particular scatter conditions used to acquire the EPID image. Moutrie et al.'s method was also adapted as described by Dancewicz et al. [7], to allow the $(\rho_e/\rho_{e,w})_{eff}$ assessment to be verified using measurements performed with a Roos ionization chamber (type 34001, PTW, Freiburg, Germany). For both the EPID measurements and the Roos chamber measurements, the water equivalent thickness of the physical sample (i.e. the thickness of water providing equivalent attenuation), t_w, was measured using comparisons with Virtual Water (Standard Imaging Inc, Middleton, USA) transmission measurements, and $(\rho_e/\rho_{e,w})_{eff}$ was calculated by division of t_w by the physical thickness of sample, t, as described by Moutrie et al and Dancewicz et al [6,7].

A reference value of ρ was defined for the sample used in this study, by measuring the mass of the sample and determining the volume of the sample. Due to the irregular shape of the sample (see Fig. 1(c)) its volume was estimated by using a high-resolution kV CT scan (small field of view and 0.5 mm slice thickness), rather than by measuring its external geometry.

2.2. Monte Carlo simulations

To characterise the dosimetric impact of the presence of the DePuy CMW 1 bone cement, percentage depth-dose profiles (PDDs) were simulated using the BEAMnrc/DOSXYZnrc Monte Carlo (MC) user codes for EGSnrc [8,9], for a 6 MV 10×10 cm^2 field produced using a validated Varian iX Clinac model [10,11]. Depth-dose profiles were simulated using four phantom geometries:

1. A homogeneous $40 \times 40 \times 40$ cm^3 phantom, consisting entirely of DePuy CMW 1 bone cement,
2. A homogeneous $40 \times 40 \times 40$ cm^3 phantom, consisting entirely of water,
3. A heterogeneous phantom, consisting of a 0.6 cm thick layer of water, above a 0.6 cm thick layer of DePuy CMW1 bone cement, above a 10 cm layer of water (to provide backscatter),
4. A heterogeneous phantom, consisting of a 0.6 cm thick layer of water, above a 0.6 cm thick layer of cortical bone ($\rho = 1.85$ g/cm^3), above a 10 cm layer of water.

The thicknesses of the layers used in the heterogeneous phantoms (phantoms 3 and 4) were chosen for consistency with skin and skull thicknesses reported in the literature [12].

To model the DePuy CMW 1 bone cement, the elemental composition was taken from vendor specifications, summarised in Table 1. Elemental composition as percentage by mass (%wt) were determined using molecular formula and molecular weight. The bone cement was added to the material definition file required by EGSnrc using this elemental composition and a default density of 1.08 g/cm^3, directly calculated from the measured mass and apparent volume in CT image of the physical sample.

2.3. Treatment dose calculations

When surgery to remove or de-bulk a cancerous lesion is undertaken

Table 1
Composition of DePuy CMW 1 bone cement.

Ingredient	Molecular Formula	% composition by mass
Solid component (40 g)		
Gentamicin sulphate	$C_{19}H_{40}N_5O_{11}S$	4.22
Polymethyl Methacrylate	$C_5O_2H_8$	84.73
Benzoyl Peroxide	$C_{14}H_{10}O_4$	1.95
Barium Sulphate	$BaSO_4$	9.10
Liquid component (20 ml, 19 g)		
Methyl Methacrylate	$C_5H_8O_2$	98.50
N,N-Dimethyl-p-toluidine	$C_9H_{13}N$	≤1.50
Hydroquinone	$C_6H_6O_2$	< 0.1

Table 2
Information regarding the treatment plans that were selected for evaluation in this study, including the treatment site, whether a bone flap was present in the planning CT or a virtual bone flap was contoured, the prescribed treatment dose and the volumes of the PTV, the contoured bone flap ("Flap") and the overlap between the PTV and the contoured bone flap ("Overlap").

Case no.	Treatment site	Bone flap	Prescription (total dose (Gy)/no. fractions)	Volumes (cm^3)		
				PTV	Flap	Overlap
1	Frontal lobe	Present	30/5	53.4	9.7	3.6
2	Frontal lobe	Present	40/15	268.4	16.0	5.9
3	Frontal lobe	Present	30/5	59.1	26.3	0.1
4	Frontal sweat gland	Present	60/30	70.0	16.5	16.5
5	Lacrimal gland	Virtual	50/20	8.8	2.2	0.9
6	Meninges	Present	54/30	23.0	17.6	4.3
7	Scalp	Virtual	50/20	34.5	11.1	4.3
8	Scalp	Virtual	60/30	195.2	33.4	13.6
9	Scalp	Virtual	60/30	175.2	57.0	6.3
10	Scalp	Present	66/33	149.1	41.3	36.1

via craniotomy, the region of bone excised may be replaced at the end of the surgical procedure if there is no cancerous involvement of the bone and if the bone has not been destroyed in the removal process. Otherwise, bone cement can be used to replace the skull bone. The removed section of the skull, whether returned or replaced with bone cement, is referred to as a "bone flap". Bone flaps are often visible in cranial radiotherapy planning CT images, due to the small gaps around their edges. See Fig. 1 (a) for an illustration of this gap and a sample contour.

For this study, ten cranial volumetric modulated arc therapy (VMAT) treatment plans were selected for investigation and recalculation, as listed in Table 2. In six of these ten cases, bone flaps were clearly identified in the planning CT images and were contoured within the treatment planning system. For each of the remaining four cases, where no bone flap was present, a "virtual bone flap" was contoured over a worst-case-scenario region of the skull, adjacent to the planning target volume (PTV). These virtual bone flaps were introduced to increase the number and range of treatment plans evaluated in this study.

For each of the treatment plans listed in Table 2, the radiotherapy treatment dose was recalculated with and without the use of a density override applied to the flap volume, in order to compare the dose calculations resulting from treating each bone flap as bone against the dose calculations resulting from treating each bone flap as approximately unit-density bone cement.

The VMAT treatments were planned using the Varian Eclipse treatment planning system, with the AAA dose calculation algorithm (version 13.7.14), for delivery with a 6 MV beam on a Varian Clinac 21iX. The study was approved by the Metro North Hospital and Health Service Human Research Ethics Committee on 30 October 2019 (reference QRBW/58067). For this retrospective study, a waiver of consent was granted by the ethics committee. The ten treatment plans are summarized in Table 2.

Table 3
Radiological characteristics of the bone cement sample (ρ and $\rho_e/\rho_{e,w}$) derived from kV CT and MV CT image data, ionization chamber measurements of $\rho_e/\rho_{e,w}$ obtained in a 6 MV treatment beam and EPID measurements of $\rho_e/\rho_{e,w}$ obtained in a 6 MV treatment beam.

Modality	Energy	ρ (g/cm^3)	$\rho_e/\rho_{e,w}$
kV CT	120 kVp	1.78 ± 0.04	1.66 ± 0.03
MV CT	3.5 MV	1.06 ± 0.04	1.04 ± 0.03
Linac with ionisation chamber	6 MV	–	1.02 ± 0.08
Linac with EPID	6 MV	–	1.08 ± 0.10

Minimum, median and maximum dose values and homogeneity index (HI, defined as $HI = [D_{2\%}–D_{98\%}]/D_{50\%}$) in the PTV were extracted from the calculated dose distributions using the Treatment and Dose Assessor (TADA) software [13,14]. A boolean difference (subtraction) operation was performed to obtain a planning target volume minus any overlapping flap volume ("PTV minus flap"), for calculation of dose-volume metrics exclusive of any dose difference in the bone flap.

3. Results

3.1. Radiological characterisation

The ρ of the bone cement sample derived from the 120 kVp CT data was 1.78 ± 0.04 g/cm^2 (see Table 3), which fell into the established range of human bone densities, 1.18 g/cm^3 to 1.92 g/cm^2 [15]. However, the results derived from the MV CT data, which were confirmed by the EPID and ionisation chamber measurements of $\rho_e/\rho_{e,w}$ in a 6 MV treatment beam (all MV results in Table 3 agreed within uncertainties), indicated that the effective $\rho_e/\rho_{e,w}$ of this bone cement in megavoltage photon energies (and therefore the effect of this bone cement on the MV treatment beam) was more similar to water or soft tissue.

The ρ determined by measurement of mass and volume was 1.08 g/cm^3, which was similarly close to unity and similar to water, and which also confirmed that the bone-like density identified in the kV CT images resulted from photoelectric enhancement in the small proportion of radiopacifier in the sample (see Table 1) and did not accurately reflect the true ρ of the sample.

3.2. Monte Carlo simulations

For the homogeneous phantom simulations (phantoms 1 and 2, as defined in Section 2.2), the difference between dose in water and dose in the bone medium was approximately 0.6% in the build-up region and 2% between depth of dose maximum and 20 cm depth, which decreased to 1.3% at 40 cm depth.

For the heterogeneous layered phantom simulations (phantoms 3 and 4, as defined in Section 2.2), the bone cement and bone flap dose percentage depth dose profiles and percentage differences are shown in Fig. 2.

Differences of 7% between the doses calculated in phantom 3 (with bone cement) and phantom 4 (with bone) were observed at the downstream interface. Differences exceeded the 0.6% combined statistical uncertainty of the Monte Carlo calculations for phantoms 3 and 4 to a depth of 0.4 cm past the flap layer, with 2% deviations observed between 0.1 and 0.3 cm depth past the flap layer.

3.3. Treatment dose calculations

Based on the results of the reference ρ measurement and the radiological characterisation of the bone cement sample (see Section 3.1), a density override of ρ = 1.08 g/cm^3 (corresponding to 13 HU for this specific kV CT calibration) was selected to each bone flap in the ten VMAT cases listed in Table 2, in order to establish the effects of correctly modelling bone cement implants according to their effective density in a MV treatment beam (see Section 2.3). Fig. 3 shows the resulting calculated differences between PTV doses (maximum, minimum and median doses in the whole PTV and the PTV with the bone flap subtracted) and differences between the homogeneity indices.

The results in Fig. 3(a) and (b) indicate that, while the use of complex VMAT treatments effectively reduces the dose discrepancy compared to the use of a single beam directed at a normal to the implant (as shown in Fig. 2), dose errors of up to 2% could nonetheless occur if the dose from a treatment involving bone cement was calculated as though the bone cement was bone rather than approximately unit-density plastic.

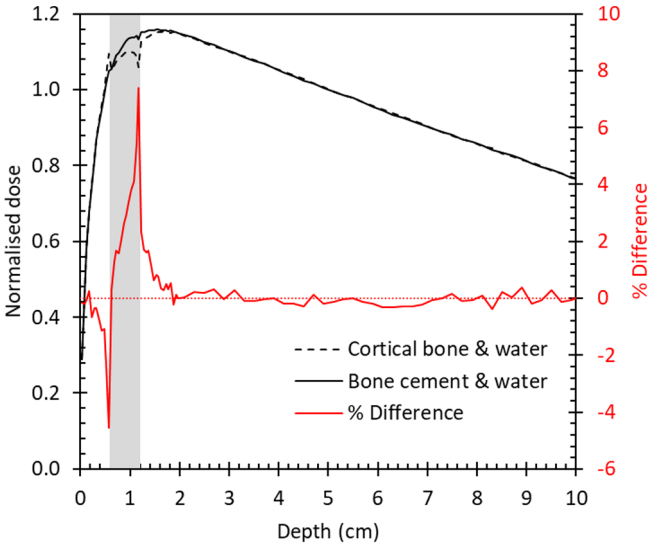

Fig. 2. Percentage depth-dose in heterogeneous layered phantom normalized to 5 cm depth, from Monte Carlo simulations of phantoms 3 and 4, as defined in Section 2.2. Area shaded grey between 0.6 and 1.2 cm depth indicates phantom region filled with either cortical bone (phantom 3) or bone cement (phantom 4), while other depths show dose calculated in the surrounding water. Red line and right-hand axis show the percentage difference between the two depth-dose results. (For interpretation of the references to colour in this figure legend, the reader is referred to the web version of this article.)

The results in Fig. 3(a) and (b) show that in the cases evaluated in this study, the doses to the PTV (defined with or without the inclusion of the bone flap overlap region) generally increased when the bone flap was overridden to match the MV effective density of bone cement. Dose differences were most dramatic for cases 9 and 10, which were both scalp treatments, whereas more equivocal results were obtained for cases 1 to 3, which were all treatments of brain tumours at various distances from the skull.

The results in Fig. 3(c) show that in most cases, the homogeneity index increased (ie. the level of dose heterogeneity in the plans increased) when the bone cement density override was used, indicating that the treatment doses calculated without the override under-estimated the dose heterogeneity in many of these cases.

4. Discussion

Plastic-based bone cements appear as bone in kV CT images but behave as plastic in MV treatment beams. There exist potential errors in dose calculations for MV radiotherapy treatments when the ρ and/or ρ_e/$\rho_{e,w}$ of plastic-based cements are incorrectly assigned in the treatment planning system, using values generated from kV CT images. Dose downstream of a plastic-based cement could be 7% higher than expected at the cement tissue interface, for a single orthogonally incident beam. Differences in target dose volume metrics averaged 0.5%, with the largest disagreement observed being 2%.

The existing literature on this subject is sparse, given that observers without access to MV imaging systems may assume that the elevated density reported by kV CT imaging systems indicates the true effect of radiopacifier materials on the MV treatment beam. Several relevant studies can be found in the area of intravenous CT contrast, where concern regarding dose calculation accuracy is generally focused on the fact that contrast agents are present during CT image acquisition but not during treatment [5], rather than on the possibility that the effects of contrast agents are over-estimated during treatment planning due to radiopacifiers causing elevated HU values in the kV CT images [16]. For example, Choi et al. calculated head-and-neck radiotherapy treatment doses using kV CT images of fifteen patients, acquired with and without administration of iodinated contrast, and showed that the dose delivered during treatment would have been up to 1% higher than planned, due to the absence of the contrast agent during treatment [5].

By contrast, and similar to the current study, when Liauw et al. observed similar differences between dose distributions calculated with and without intravenous contrast included in the kV CT data for a further five patients, their conclusion acknowledged that bright regions in planning CT images (and resulting effect on treatment planning dose calculations) from contrast agents radiopacified with iodine, calcium and barium was due to photoelectric enhancement in the kV imaging beam, while these materials would have much less effect on the MV treatment beam, where the dominant interaction is Compton scattering [16].

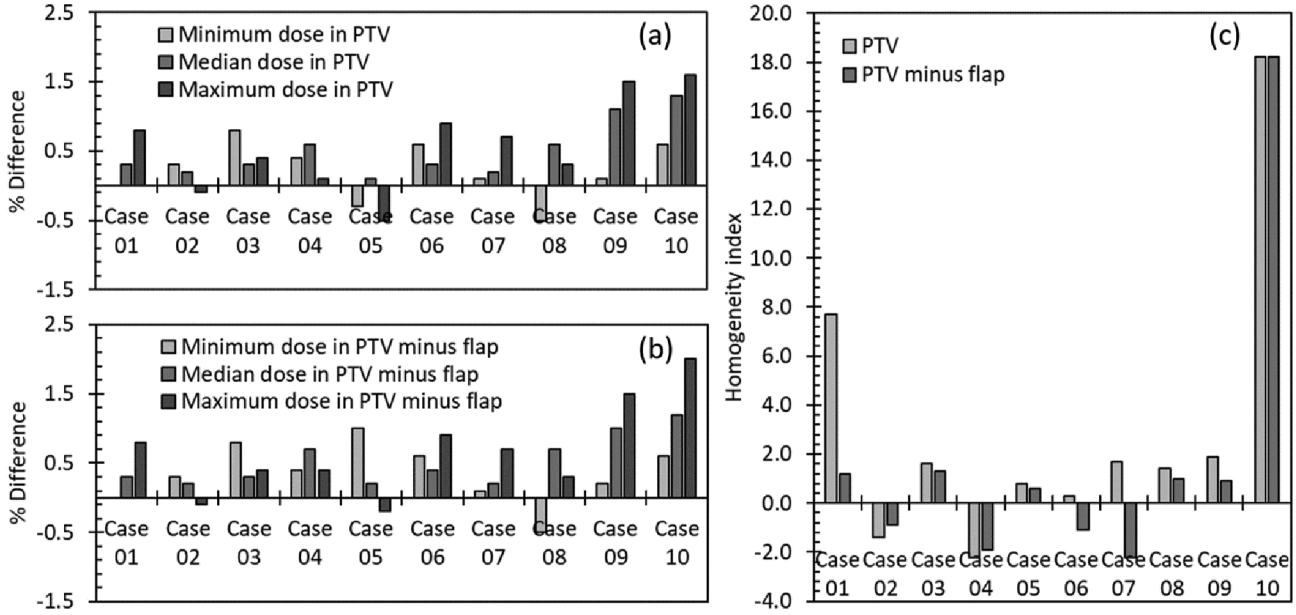

Fig. 3. Percentage differences between dose metrics calculated with bone flap modelled as bone and with bone flap modelled as bone cement, calculated in either (a) the PTV or (b) the PTV with any overlap with the bone flap subtracted, alongside (c) the percentage differences between homogeneity indices calculated with bone flap modelled as bone and with bone flap modelled as bone cement, for the ten VMAT treatment cases listed in Table 2.

The key reference in this area is Ramm et al.'s early study of barium-radiopacified boluses in water, which frankly acknowledged that the "treatment planning system erroneously takes [the radiopacified boluses] for high density tissue" and pointed out that the treatment planning system's over-estimation of the beam attenuating effects of the radiopacified materials would lead to treatment plans that under-estimated the dose delivered to patients [4]. While Ramm et al.'s study used dose calculations over a course (5 mm^3) dose grid, which hid the effects of build-up and scatter that are apparent in Fig. 2, Ramm et al. were nonetheless able to identify dose differences of up to 7.4% for single 6 MV photon beams, which were reduced to 3.2% by the use of parallel-opposed beams [4].

The major limitation of the current study was our use of Monte Carlo simulations that considered only 10 × 10 cm^2 6 MV photon beams orthogonally incident on rectilinear approximations of cranial anatomy, simple layers representing scalp, bone cement and water. Further Monte Carlo investigations are advisable, to establish the extent to which these results might vary for tangential beams, small fields, electron beams, kilovoltage X-ray beams and other phantom geometries.

The results of the recalculations of clinical treatment dose included in this study suggest that for treatments exploiting multiple angles of incidence, i.e. VMAT treatments, dose deviations arising from the presence of bone cement are reduced, particularly for intracranial volumes, due to the comparatively large proportion of the dose that is delivered from gantry angles that do not enter the target through the specific region of the skull replaced by bone cement. The largest dose deviations were observed for scalp treatments, where thin and slightly concave targets directly overlie the cranial bones and bone cement.

For post-craniotomy patients presenting for cranial radiotherapy, it is not necessarily obvious that a plastic-based cement is present, on visual inspection of kV CT simulation or typical kV cone-beam CT treatment images. For treatments of volumes near a potential bone cement insert (i.e. near a visible bone flap), the following steps are advisable to reduce the risk of erroneous dose calculations:

The appearance of the bone flap in the CT image should be visually inspected, to look for any evidence of artificial material (e.g. irregular air cavities, different texture or CT number compared to surrounding bone). Patient records should be inspected and/or information should be sought from the surgical team, to determine whether bone cement was used. An MV radiograph or MV CT of the anatomy (e.g. using an EPID [17]) should be performed, to identify whether an unexpected unit-density region is present within the skull. The weighting of beams/beamlets that deposit dose downstream of the bone flap should be minimized, by increasing the number of treatment beams or by using arcs, including VMAT arcs. Care should be taken when considering dosimetric trade-offs based on maximum dose or PTV homogeneity as these values are most affected by the uncorrected presence of bone cement.

In conclusion, additional care should be taken when treating patients where plastic-based bone cements may be present, as the radiological properties of these materials may appear similar to bone in kV treatment planning CT images, but vary significantly for MV treatment beam energies.

Declaration of Competing Interest

The authors declare that they have no known competing financial interests or personal relationships that could have appeared to influence the work reported in this paper.

Acknowledgements

SBC's contributions to the paper were supported by the MNHHS and QUT Herston Biofabrication Institute Cancer Care Services program. The authors wish to thank radiation oncology, radiation therapy and medical physics staff for assistance with the study, in particular Dr. Paul Charles and Naasiha Cassim; and Dr. Darryl Dunn for assistance in acquiring the bone cement sample.

References

[1] Dunne N, Clements J, Wang J-S. Chapter 8 – Acrylic cements for bone fixation in joint replacement. Joint Replacement Technology, 2nd ed.; 2014.
[2] Artola A, Gurruchaga M, Vázquez B, San Román J, Goñi I. Elimination of barium sulphate from acrylic bone cements. Use of two iodine-containing monomers. Biomaterials 2003;24:4071–80. https://doi.org/10.1016/S0142-9612(03)00298-9.
[3] Kairn T, Zahrani M, Cassim N, Livingstone AG, Charles PH, Crowe SB. Quasi-simultaneous 3D printing of muscle-, lung- and bone-equivalent media: a proof-of-concept study. Phys Eng Sci Med 2020; in press. https://doi.org/10.1007/s13246-020-00864-5.
[4] Ramm U, Damrau M, Mose S, Manegold KH, Rahl CG, Böttcher H-D. Influence of CT contrast agents on dose calculations in a 3D treatment planning system. Phys Med Biol 2001;2001(46):2631. https://doi.org/10.1088/0031-9155/46/10/308.
[5] Choi Y, Kim JK, Lee HS, Hur WJ, Hong YS, Park S, et al. Influence of intravenous contrast agent on dose calculations of intensity modulated radiation therapy plans for head and neck cancer. Radiother Oncol 2006;81:158–62. https://doi.org/10.1016/j.radonc.2006.09.010.
[6] Moutrie V, Kairn T, Rosenfeld A, Charles PH. Use of a megavoltage electronic portal imaging device to identify prosthetic materials. Australas Phys Eng Sci Med 2015;38:93–100. https://doi.org/10.1007/s13246-015-0327-8.
[7] Dancewicz OL, Sylvander SR, Markwell TS, Crowe SB, Trapp JV. Radiological properties of 3D printed materials in kilovoltage and megavoltage photon beams. Phys Med 2017;38:111–8. https://doi.org/10.1016/j.ejmp.2017.05.051.
[8] Rogers DWO, Faddegon BA, Ding GX, Ma C-M, We J, Mackie TR. BEAM: a Monte Carlo code to simulate radiotherapy treatment units. Med Phys 1995;22:503–24. https://doi.org/10.1118/1.597552.
[9] Kawrakow I, Mainegra-Hing E, Rogers DWO, Tessier F, Walters BRB. The EGSnrc Code System: Monte Carlo simulation of electron and photon transport. Technical Report PIRS-701. National Research Council Canada; 2017.
[10] Kairn T, Crowe SB, Charles PH, Trapp JV. Using narrow beam profiles to quantify focal spot size, for accurate Monte Carlo simulations of SRS/SRT systems. J Phys Conf Ser 2014;489:012014https://doi.org/10.1088/1742-6596/489/1/012014.
[11] Livingstone AG, Francis K. O51 Clinical implementation of an automated Monte Carlo dose verification system. Australas Phys Eng Sci Med 2018;41:282–3.
[12] Haeussinger FB, Heinzel S, Hahn T, Schecklmann M, Ehlis AC, Fallgatter AJ. Simulation of near-infrared light absorption considering individual head and prefrontal cortex anatomy: implications for optical neuroimaging. PLoS ONE 2011;6:e26377https://doi.org/10.1371/journal.pone.0026377.
[13] Crowe SB, Kairn T, Middlebrook N, Hill B, Christie DRH, Knight RT, Kenny J, Langton CM, Trapp JV. Retrospective evaluation of dosimetric quality for prostate carcinomas treated with 3D conformal, intensity-modulated and volumetric-modulated arc radiotherapy. J Med Radiat Sci 2013;60:131–8. https://onlinelibrary.wiley.com/doi/full/10.1002/jmrs.24.
[14] Kairn T, Crowe SB. Retrospective analysis of breast radiotherapy treatment plans: Curating the 'non-curated'. J Med Imag Radiat Oncol 2019;63:517–29. https://onlinelibrary.wiley.com/doi/10.1111/1754-9485.12892.
[15] White DR, Booz J, Griffith RV, Spokas JJ, Wilson IJ. ICRU Report 44 Tissue Substitutes in Radiation Dosimetry and Measurement. Journal of the International Commission on Radiation Units and Measurements, 1989;os23:NP. https://doi.org/10.1093/jicru/os23.1.Report44.
[16] Liauw SL, Amdur RJ, Mendenhall WM, Palta J, Kim S. The effect of intravenous contrast on intensity-modulated radiation therapy dose calculations for head and neck cancer. Am J Clin Oncol 2005;28(5):456–9. https://doi.org/10.1097/01.coc.0000170796.89560.02.
[17] Markwell T, Perera L, Trapp J, Fielding A. Evaluation of MegaVoltage Cone Beam CT image quality with an unmodified Elekta Precise Linac and EPID: a feasibility study. Australas Phys Eng Sci Med 2014;37:291–302. https://doi.org/10.1007/s13246-014-0258-9.